

# Theoretical Limits of Backscatter Communications

Clemens Korn, Joerg Robert, Tobias Dräger

This work has been submitted to the IEEE for possible publication. Copyright may be transferred without notice, after which this version may no longer be accessible.

**Abstract**—Backscatter communication is a hot candidate for future IoT systems. It offers the possibility for connectivity with tiny amounts of energy that can be easily obtained from energy harvesting. This is possible as backscatter devices do not actively transmit electromagnetic waves. Instead they only reflect existing electromagnetic waves by changing the antenna load. This fact leads to significant differences compared to classical communication wrt. the modulation schemes and achievable data rates. However, to our best knowledge nobody has so far systematically analyzed the achievable data rates and transmit ranges for different parameter configurations. Within this paper we derive theoretical bounds for backscatter communications based on classical information theory. We then use these bounds to analyze how different parameters – e.g. the distance, the frequency, or the transmit power – affect the achievable data rates. The bounds are derived for mono-static configuration, as well as for bi-static configurations. This allows feasibility analyses for different use-cases that are currently discussed in 3GPP and IEEE 802.

**Index Terms**—Backscatter communication, IoT, low-power communication, ambient backscatter, wireless sensor networks

## I. INTRODUCTION

Backscatter-based radio communication is already a proven and well-established technology, e.g. in UHF-RFID (Ultra High Frequency Radio Identification) [1]. However, it is also a hot candidate for future IoT (Internet of Things) systems [2]. This is particularly the case for passive IoT systems and sensors. These systems are typically not equipped with a powerful battery and have to harvest their complete energy. Hence, they can only afford to spend very tiny amounts of energy for RF (Radio Frequency) communication. These passive devices are currently discussed for future 6G communication networks [3], [4], and as a topic for a possible new 3GPP Study Item “Ambient IoT”. Also in IEEE 802.11 (WiFi) there currently exists the “Ambient Power (AMP)” Technical Interest Group.

Backscatter devices are not an active transmitter of electromagnetic waves. Instead, they are reflecting already existing electromagnetic waves by changing the impedance of their antenna, e.g. they switch the antenna load between open and short [5]. This leads to a very tiny power consumption for the backscatter devices, mainly due to two reasons: First, no

amplifier is required inside the backscatter device. Secondly, the backscatter device does not need any high-precision oscillator. It does not have to generate a high frequency signal at the carrier frequency, but only a modulation at the symbol rate, which normally is several magnitudes smaller than the carrier frequency. An example for the power consumption of a backscatter modulator is e.g. presented in [6]. The power consumption only depends on the data rate, but not on the carrier frequency. This shows, that backscattering is particularly suited for all kinds of use-cases where small amounts of data have to be transmitted over a limited range and where low power consumption and low complexity at the transmitter side is required.

The signal that is backscattered and modulated by the passive device can either origin from a dedicated source, or from an ambient source. Relying on a dedicated source is the traditional approach for backscattering. Here, a signal (typically a continuous wave) is radiated with the aim of providing a carrier signal that can be backscattered by a device. Usually, the signal from the dedicated source is also used for powering the backscatter device, as done in case of passive UHF-RFID [7]. Another approach that recently got increasing attention in research is to use an ambient source [8]. Here, the backscatter device uses already existing signals from other radio systems that have not been radiated for backscattering purposes. Examples are radio broadcast or signals from mobile cellular networks.

There already exists a plethora of work where ambient backscattering has been implemented. In [9], measurement results are presented for ambient backscattering using signals from FM Radio, ATSC Digital TV, CMDA2000, or UMTS. In [10], LoRa signals were used while [11] uses Bluetooth signals. FM broadcast signals were e.g. used in [12], [13], [14], while WiFi signals were used in [15], [16], [17]. Finally, generic OFDM (Orthogonal Frequency Division Multiplex) signals were used in [18], [19].

Further, there are papers that theoretically investigate some aspects of the expected performance of backscattering. The link budget is analyzed in [20] and [21], while [22] provides some insight on the achievable data rate as a function of the signal-to-noise ratio (SNR). Considering multiple users, the channel capacity and outage performance is investigated in [23], [24] and [25]. However, to our best knowledge no detailed extensive theoretical analysis on the effects of different parameters has been performed so far.

Therefore, in our work we investigate the theoretical limits of backscattering communications in terms of maximum achievable payload data rate based on Shannon’s communication theory. This paper is structured as follows. Sec. II presents the channel model with two different backscattering

Clemens Korn is with the Dependable M2M Research Group, Technische Universitaet Ilmenau, Germany, and with the Fraunhofer IIS, Fraunhofer Institute for Integrated Circuits IIS, Nuremberg, Germany, e-mail: clemens.korn@tu-ilmenau.de

Joerg Robert is with the Dependable M2M Research Group, Technische Universitaet Ilmenau, Germany, and with the Fraunhofer IIS, Fraunhofer Institute for Integrated Circuits IIS, Erlangen, Germany, e-mail: joerg.robert@ieee.org

Tobias Dräger is with the Fraunhofer IIS, Fraunhofer Institute for Integrated Circuits IIS, Self-Powered Radio Systems Department, Erlangen, Germany, e-mail: tobias.draeger@iis.fraunhofer.de

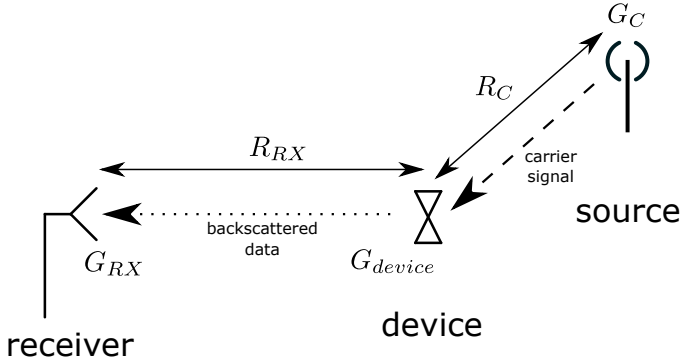


Fig. 1. Channel model of the bi-static configuration: The path of the carrier signal from carrier signal source to backscatter device is illustrated by the dashed arrow, while the path of the backscattered signal from backscatter device to the receiver is illustrated by the dotted arrow.

configurations, a bi-static and a mono-static one. Based on these, the theoretical bounds of backscatter based communications are derived in Sec. III. In Sec. IV, we show how various system parameters influence the bound for the data rate. Finally, Sec. V shows a practical example and Sec. VI concludes this document.

## II. BACKSCATTER CHANNEL MODEL

In this section, we present our channel model for the later following investigations. This includes the backscattering setup, the path loss model, and the noise.

### A. General Assumptions

We are focusing on the theoretical bounds. Consequently, we always assume perfect conditions, which may not be reachable in real systems. We also do not care about the type of signal that we use for the backscatter modulation. It is only defined by its power  $P_C$ . Further, we assume a correlation receiver [26]. Throughout this document the passive device backscatters 100% of the received signal power, which corresponds to a backscatter efficiency of  $\mu = 1$ . This also means that we ignore potential losses caused by the energy harvesting of the device, as e.g. done by passive UHF-RFID systems [5], [27]. Further, we assume that the signals are transmitted via line-of-sight and that RX and TX antennas are always perfectly directed towards each other during the communication. Finally, we assume that the performance of the receiver is not affected by the original carrier signal generated by the source, which is a typical problem in practical scenarios [5].

### B. Backscatter Configurations

Generally, there exist two different backscattering configurations, i.e. the bi-static and the mono-static configuration.

1) *Bi-static Configuration*: Fig. 1 shows the bi-static configuration. A high-frequency radiator (source) transmits the carrier signal to the backscatter device. The transmit power of the carrier source is given by  $P_C$ . The backscatter device then backscatters the signal to the receiver. The configuration is called bi-static, as the source and receiver do not use the same antenna.

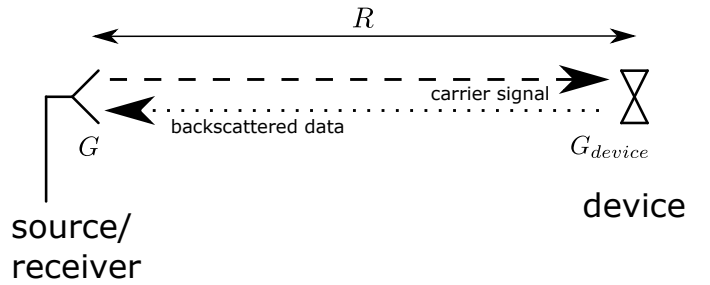


Fig. 2. Channel model of the mono-static setup: The source/receiver transmits a carrier signal to the backscatter device (dashed arrow), which then backscatters it back to the source/receiver (dotted arrow).

The bi-static configuration is the typical configuration for ambient sources, as the source could be a cellular network station. However, it can also be used in case of dedicated sources for the backscattering signal, as it does not suffer due to problem of simultaneous transmission and reception from the same antenna.

In the following,  $R_C$  denotes the distance from the source to the backscatter device, and  $R_{RX}$  denotes the distance between the backscatter device and the receiver. Further, the antenna gain of the source is given by  $G_C$ ,  $G_{device}$  defines the antenna gain of the backscatter device, and  $G_{RX}$  is the antenna gain of the receiver.

A relevant factor for the further calculations is the EIRP (effective isotropic radiated power)  $P_{C,EIRP} = P_C G_C$  of the source, as the maximum EIRP is typically limited by the frequency regulation.

2) *Mono-static Configuration*: Fig. 4 shows the mono-static configuration, where the source and the receiver use the same antenna. This simplifies the calculations compared to the bi-static case, as  $R = R_C = R_{RX}$ . Further, we can assume identical antenna gains for the source and the reception antenna, i.e.  $G = G_C = G_{RX}$ .

### C. Path Loss Model

As aforementioned, we focus on theoretical limits. Therefore, we neglect channel conditions such as fading, shadowing, diffraction, and interference. Instead, we describe the effects of the channel only by means of the free-space path loss. Then, the power at the antenna output of the passive device is given by [26]:

$$P_{RX,device} = G_C G_{device} \left( \frac{c_0}{4\pi R_C f_c} \right)^2 P_C, \quad (1)$$

where  $P_C$  is the transmit power of the carrier signal transmitted by the source,  $c_0$  is the speed of light, and  $f_c$  is the carrier frequency. We assume a system where the backscatter device reflects the received power with efficiency  $\mu$ . This means the transmit power of the backscatter device  $P_{TX,device}$  is given by  $P_{TX,device} = \mu P_{RX,device}$ . Then, the power at the output of the receiver antenna is given by:

$$P_{RX} = G_{RX} G_{device} \left( \frac{c_0}{4\pi R_B f_c} \right)^2 \mu P_{RX,device}. \quad (2)$$

Using (1) in (2) yields the received signal power  $P_{RX,bs}$  at the receiver in a bi-static setup, which is:

$$P_{RX,bs} = G_{RX} G_C G_{device}^2 \left( \frac{c_0}{4\pi f_c} \right)^4 \frac{\mu P_C}{R_{RX}^2 R_C^2}. \quad (3)$$

In case of a mono-static setup, we use  $R = R_{RX} = R_C$  and  $G = G_C = G_{RX}$ . Then, (3) simplifies to:

$$P_{RX,ms} = G^2 G_{device}^2 \left( \frac{c_0}{4\pi R f_c} \right)^4 \mu P_C, \quad (4)$$

where  $P_{RX,ms}$  is the received signal power at the receiver in the mono-static case.

#### D. Noise

In order to model the noise we assume thermal noise with an ambient temperature of  $T = 300$  K. This leads to a noise power spectral density  $N_{0,th} = -174$  dBm/Hz [28]. The noise is characterized by additive white Gaussian noise.

The total noise power  $N$  is then given by  $N = N_0 W$ , where  $W$  is the bandwidth of the received signal and  $N_0$  is the one-sided noise power spectral density.  $N_0$  is given by  $N_0 = N_{0,th} F$ , where  $F$  is the receiver's noise figure. Therefore, the received signal-to-noise ratio (SNR) is given by:

$$\text{SNR} = \frac{P_{RX}}{N_{0,th} F W}, \quad (5)$$

where  $P_{RX}$  is defined by (3) for the bi-static configuration, and by (4) for the mono-static configuration.

Assuming a correlation receiver, we can express the SNR also by the  $E_b/N_0$  [26]. The ratio between the received energy per bit  $E_b$ , and the one-sided noise power spectral density at the receiver  $N_0$ , in our system is obtained by considering that  $E_b = P_{RX}/r_b$ , where  $r_b$  is the data rate, and  $N_0 = N_{0,th} F$ , which yields:

$$\frac{E_b}{N_0} = \frac{P_{RX}}{r_b N_{0,th} F}. \quad (6)$$

We are focusing on the theoretical bounds. Consequently, we will assume a noise figure of  $F = 1$  (i.e. 0 dB) in Sec. IV. This means we assume a perfect receiver that does not add any additional noise [28].

#### E. Carrier Frequency, Bandwidth and Transmission Power

Due to the frequency regulation, the system parameters cannot be randomly selected, especially in case of non-ambient backscattering. Available bands for transmitting the carrier signal are the license-exempt ISM (Industrial, Scientific and Medical) or SRD (Short Range Devices) bands. As the backscatter signal typically has to remain in these bands, its maximum bandwidth is limited.

For the US, the FCC (Federal Communications Commission) assigns three ISM (Industrial, Scientific and Medical) bands around 915 MHz (with 26 MHz bandwidth), 2.4 GHz (with 83.5 MHz bandwidth), and 5.8 GHz (with 125 MHz bandwidth) in FCC Title 47, §15.247 [29]. The radiated electrical power in these bands is limited to 1 W with an antenna gain of up to 6 dBi, leading to a maximum EIRP (effective isotropic radiated power) of 4 W (36 dBm).

For Europe, the ETSI (European Telecommunications Standards Institute) assigns two frequency bands for backscatter communications:

- ETSI EN 302 208 [30] defines a "lower band" at 868 MHz with an ERP<sup>1</sup> (effective radiated power) of 2 W in a bandwidth of 200 kHz, and an "upper band" at 915 MHz with an ERP of 2 W in a bandwidth of 400 kHz. The latter, however, is only available in few European countries. The ERP of 2 W is equivalent to an EIRP of 3.28 W.
- ETSI EN 300 440 [31] assigns a 8 MHz wide band at 2.4 GHz with an EIRP of 500 mW, or an EIRP of 4 W (with very strict restrictions to fixed indoor setups).

Backscatter communication could also be used in licensed frequency bands. An example is the use of FM radio or cellular networks signals as ambient carrier signals. However, there currently exist no specific frequency bands, channel bandwidths, or power limitations. Therefore, we will mainly focus on the parameters available for license-exempt frequency bands.

### III. DERIVATION OF THE THEORETICAL BOUND

Within this section we will derive the theoretical bounds for different system assumptions.

#### A. Absolute Bound

According to Shannon's coding theory, error-free communication in the AWGN (additive white Gaussian noise) channel is only possible if  $E_b/N_{0,min} \geq \ln(2)$  (or  $\geq -1.59$  dB) [26]. It has to be noted that this bound practically assumes an infinite channel bandwidth  $W$ . Considering this in (6), and solving for  $r_b$  obtains the theoretical bound  $C_\infty$  for the data rate in the infinite bandwidth channel with  $r_b \leq C_\infty$ :

$$C_\infty = \frac{P_{RX}}{N_{0,th} F \ln(2)}, \quad (7)$$

where  $F$  is the noise figure, and  $P_{RX}$  is given by (3) for the bi-static, and by (4) for the mono-static configuration. We will call  $C_\infty$  the "absolute bound" as it assumes an infinite bandwidth.

#### B. Bandwidth-limited Bound

However, (7) is only valid for systems with an infinite channel bandwidth  $W$ , which may not be possible due to the frequency regulation or practical aspects. For systems with limited bandwidth, we have to use the capacity  $C_W$  in the band-limited AWGN channel with input power constraint, which is given by [26]:

$$C_W = W \log_2(1 + \text{SNR}). \quad (8)$$

This bound depends on the bandwidth and on the SNR, which in our case is given by (5). Therefore, using (5) in (8) yields the bound for the achievable data rate  $r_b \leq C_W$  in the band-limited channel. It is given by:

<sup>1</sup>The ERP is the antenna gain wrt. a half-wave dipole antenna. 1 W ERP is equivalent to 1.64 W EIRP.

$$C_W = W \log_2 \left( 1 + \frac{P_{RX}}{N_{0,th}FW} \right), \quad (9)$$

where  $P_{RX}$  is again given by (3) for the bi-static, and by (4) for the mono-static configuration. We will call  $C_W$  the bandwidth-limited bound.

### C. Effects of Realistic Channel Coding

If realistic channel coding is applied to the transmission, there will be additional losses compared to the bounds  $C_\infty$  and  $C_W$ . The capacity equations used in the previous sections assume an infinite payload data length [32]. However, the typical information block size will be much smaller for typical backscatter scenarios. Therefore, the limited code word length introduces an additional loss given by the so-called Sphere Packing Bound. This topic is well-discussed in [32], where [32, Fig. 2] shows the resulting losses compared to the capacity for a word error-rate of  $10^{-4}$ . The loss wrt. the capacity is more than 8 dB if a single payload bit is transmitted. For an information block size of 100 bits we still have a loss of more than 2 dB. Furthermore, also the losses due to imperfect forward error correction codes have to be taken into account. However, as we are focusing on the maximum theoretical capacity, we will not consider the loss due to realistic channel coding within the remaining part of this document.

## IV. ACHIEVABLE DATA RATES FOR DIFFERENT SYSTEM CONFIGURATIONS

In this section we will examine the influence of different system parameters on the theoretical capacities. This means we assume an infinite information block size. Also, we assume a noise figure  $F = 0$  dB, which characterizes the optimum receiver. For the passive device we assume a backscatter efficiency  $\mu = 1$ , which characterizes a perfect backscatter device.

As the orientation of the passive backscatter device is unknown in most cases, it is not useful to equip them with directive antennas. Consequently, we assume a half-wave dipole with an antenna gain of  $G_{device} = 2.15$  dBi. For the source/receiver antenna we assume an antenna gain of 8 dBi, which is a typical value for UHF-RFID antennas. As the frequency regulation limits the maximum EIRP to 4 W (36 dBm), we set the transmit power to  $P_C = 0.63$  W (28 dBm). Furthermore, we assume a carrier frequency of  $f_c = 900$  MHz. Finally, we assume a mono-static backscatter configuration if not stated otherwise.

### A. Influence of the SNR

As a first step, we show the influence of the SNR on the absolute bound the bandwidth-limited bound  $C_W$  for a given bandwidth  $W = 400$  kHz.

Fig. 3 shows a steep increase for the maximum data rate  $r_b$  if  $\text{SNR} < 0$  dB, i.e.  $\text{SNR} < 1$  in the linear case. This behavior arises from the log-term in (8) and (9). This term can be approximated by  $\log_2(1+x) \sim x$ , which means (7) and (9) are approximately identical. This results in a linear increase with the SNR.

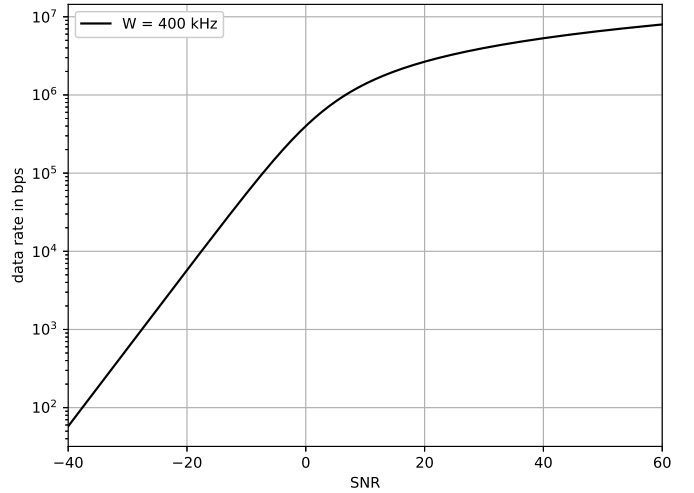


Fig. 3. Maximum data rate  $r_b$  as a function of the SNR for the absolute bound and the bandwidth-limited bound with  $W = 400$  kHz.

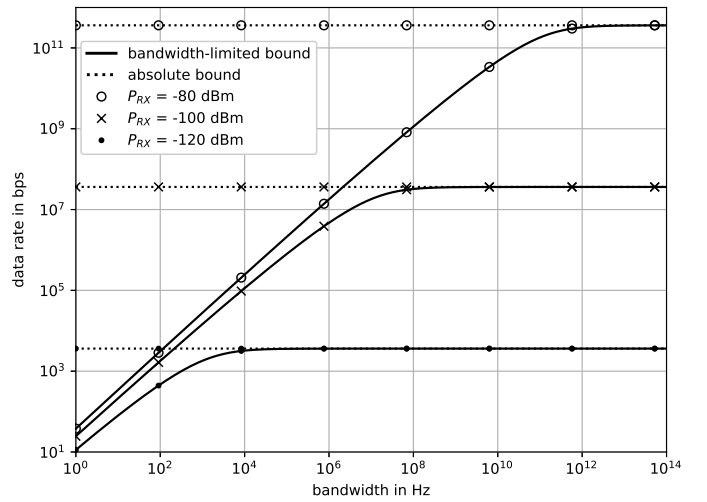


Fig. 4. Bound for the maximum data rate  $r_b$  as a function of the bandwidth  $W$  for various signal powers  $P_{RX}$ , assuming  $F = 0$  dBm and  $N_{0,th} = -174$  dBm/Hz.

For further increasing SNR the 1 in the log-term becomes negligible, and the bandwidth limitation comes into effect. In this case we get  $\log_2(1+x) \sim 10 \log_{10} x$ , where  $10 \log_{10} x$  is the dB-value of  $x$ . Consequently, the capacity  $C_W$  scales linearly with the dB-value of the SNR. The actual transition point depends on the ratio of  $P_{RX}/(N_{0,th}FW)$  in (9). A higher bandwidth  $W$  shifts the transition point to higher data rates.

### B. Influence of the Signal Bandwidth

Fig. 4 shows the bandwidth-limited bound for the maximum data rate  $r_b$  in as a function of the bandwidth  $W$  for different signal reception powers  $P_{RX}$ . As dotted lines show the absolute bounds assuming infinite bandwidth. We can see that the bandwidth-limited bound for the data rate increases with increasing bandwidth until a certain point. After that point there is no further increase and the bandwidth-limited bound approximates to the absolute bound. This is the same effect

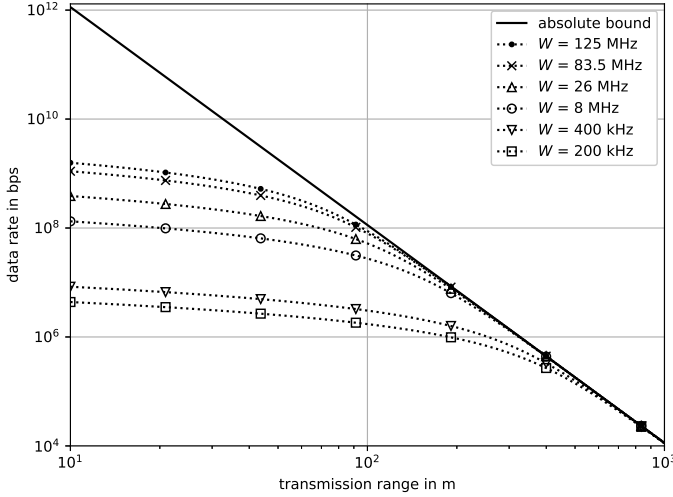


Fig. 5. Maximum data rate  $r_b$  in a mono-static setup as a function of the transmission range  $R$ . The solid curve shows the absolute bound  $C_\infty$ , while non-solid curves show the bound  $C_W$  for the bandwidth-limited cases.

that we already discussed in Section IV-A. It is the point, where the SNR in (8) reaches 0 dB. The location of this point depends both on the bandwidth and the power of the received signal. It is reached later for higher signal powers. Left hand side of this point the bandwidth  $W$  is the main limiting factor, resulting from the log-term in (8). On the right hand side of this point the bandwidth  $W$  is so high that we can again approximate  $\log_2(1+x) \approx x$  as  $x < 1$ . Hence, the SNR, or equivalently the received signal power  $P_{RX}$  in (9), becomes the limiting factor.

### C. Influence of the Distance

The effect of the distance  $R$  is of high interest for many applications. Fig. 5 shows the bandwidth-limited  $C_W$  bound for the maximum data rate  $r_b$  for different bandwidths as a function of the distance  $R$ . In addition, the solid curve shows the absolute bound  $C_\infty$  assuming an infinite bandwidth.

The figure shows that the data rate for bandwidth-limited systems only decreases slowly as the distance increases. This is again in the region where  $\text{SNR} > 0$  dB, i.e. the log-term limits the maximum data rate. For higher distances we get into the region  $\text{SNR} < 0$  dB, i.e. where we can approximate the log-term by  $\log_2(1+x) \approx x$ . In this region, the system is not limited by the bandwidth anymore, but by the low received signal power  $P_{RX}$ . This also explains the full overlap with the absolute bound  $C_\infty$ . In this region doubling the distance decreases the data rate by the factor 16. The reason is given in (4), as  $P_{RX} \sim R^{-4}$ .

### D. Influence of Carrier Signal Power

An important system parameter in real systems is the carrier signal power  $P_C$ , which is typically given by the frequency regulation. Eq. (5) shows that it influences the received SNR linearly. Therefore, every increase of the carrier signal power by 1 dB increases also the  $P_{RX}$  – and equivalently the SNR – by 1 dB.

Fig. 6 shows the influence of  $P_C$  on the maximum data rate  $r_b$ . We again assume the mono-static configuration. Again

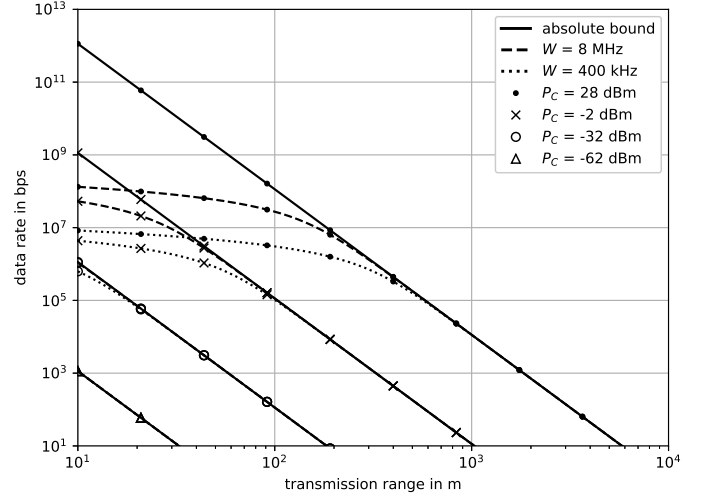


Fig. 6. Maximum data rate  $r_b$  in a mono-static setup as a function of the transmission range for different carrier signals powers  $P_C$ . The solid curves show the absolute bound  $C_\infty$ , while the dotted curves show the bandwidth-limited bound  $C_W$ .

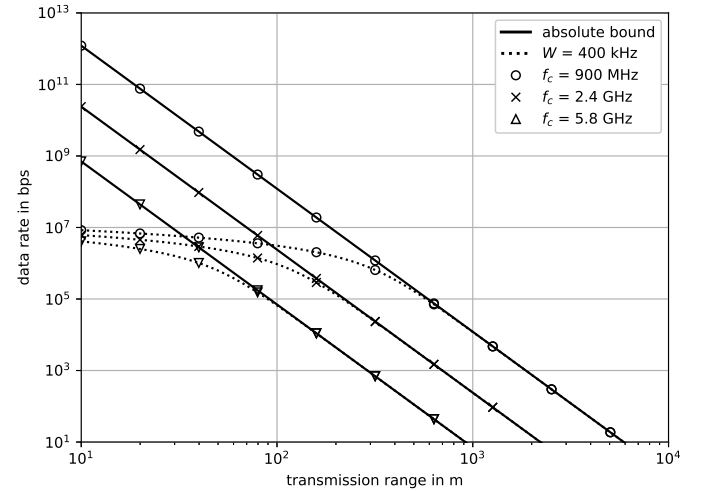


Fig. 7. Maximum bound for the data rate  $r_b$  in a mono-static setup as a function of the transmission range  $R$  for different carrier frequencies  $f_c$ . The solid curves show the absolute bound  $C_\infty$ , while the dotted curves show the bandwidth-limited bound  $C_W$  with  $W = 400$  kHz.

we can observe the bandwidth limited regions for high SNR, indicated by the non-solid lines. For the SNR limited region increasing the  $P_C$  by 30 dB increases the data rate by the factor 1000. The effect is much smaller for the bandwidth limited region. Further, this figure shows that the bandwidth  $W$  causes a practical upper limit for the achievable data rate, which is at around 150 Mbps for  $W = 8$  MHz, and 10 Mbps for  $W = 400$  kHz.

### E. Influence of the Carrier Frequency

Now we will analyze the effect of the carrier frequency  $f_c$ . Fig. 7 shows the absolute bound for the data rate  $r_b$  for the ISM band frequencies  $f_c = 915$  MHz,  $f_c = 2.4$  GHz, and  $f_c = 5.8$  GHz. The dotted line further shows the maximum data rate in case of a bandwidth of  $W = 400$  kHz. We again use the mono-static configuration. In the bandwidth

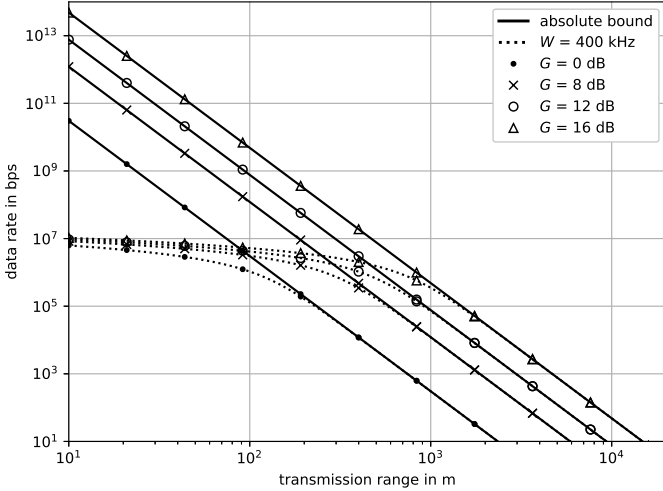


Fig. 8. Maximum data rate  $r_b$  as a function of the transmission range  $R$  for various antenna gains  $G$ . The solid curves show the absolute bound  $C_\infty$ , while the dotted curves show the bandwidth-limited bound  $C_W$  with  $W = 400$  kHz.

limited case the maximum data rate again converges to approx. 10 Mbps. However, a strong impact of the carrier frequency on the range  $R$  is visible, as  $P_{RX} \sim f_c^{-4}$ . Consequently, smaller frequencies are more suitable for backscatter modulation, as they support higher ranges. The reason for this effect is hidden in the free-space path loss equation. As we assume an omnidirectional pattern of the antenna of the passive device, we are limited to small antenna gains  $G_{device}$ . Consequently, increasing the carrier frequency will reduce the antenna size. Hence, this will also reduce the effective antenna aperture (also called radar cross section) that reflects the carrier signal to the receiver [28].

#### F. Influence of the Antenna Gain

Increasing the antenna gains is a classical method to improve the received signal level, and hence the data rate or the distance. Here we again assume the mono-static configuration. Consequently, the antenna gain at the source and the receiver are identical, i.e.  $G = G_{RX} = G_C$ . The antenna gain of the passive device is not modified.

Fig. 8 shows the achievable maximum data rates for different antenna gains  $G$  as function of the distance  $R$ . Again we assume a transmit carrier power of  $P_C = 28$  dBm. Increasing the antenna gain helps on the transmit and receive side. An increase of 1 dB improves the rate by the factor 1.58, or increases the range by factor 1.12.

However, for practical applications we have to take the frequency regulation into account that limits the EIRP  $P_{C,EIRP} = P_C G$  (cf. Sec. II-E). Consequently,  $P_C$  has to be reduced to meet the maximum allowed EIRP of e.g.  $P_{C,EIRP} = 36$  dBm. This effectively means that an additional antenna gain will only help on the receiver side. An additional antenna gain of 1 dB will then improve the rate only by factor  $\sqrt{1.58} = 1.26$ , and the range by factor  $\sqrt{1.12} = 1.06$ .

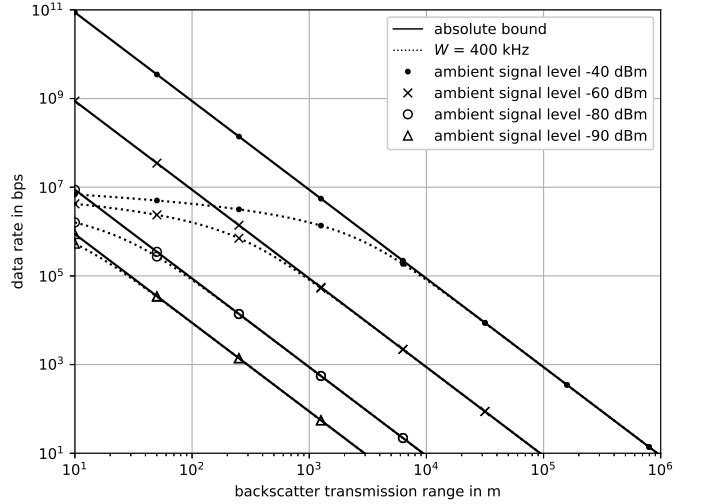


Fig. 9. Maximum data rate  $r_b$  for a bi-static setup as a function of the backscatter transmission range  $R_{RX}$  for different ambient signal levels at a carrier frequency of  $f_c = 200$  MHz. The solid curves show the absolute bound  $C_\infty$ , while the dotted curves show the bandwidth-limited bound  $C_W$  with  $W = 400$  kHz.

#### G. Influence of the Distance in an Ambient Backscattering Configuration

Here, we show the theoretical limits for ambient backscattering considering Digital Audio Broadcasting (DAB) signals as ambient carrier signal.

DAB is a radio broadcast standard for digital radio service which radiates a constant data stream without pauses. DAB systems are planned in a way that enables a sufficient signal level for receiving DAB radio service over a wide area in regions where it is deployed. The guidelines for planning DAB networks of the European Broadcasting Union (EBU) [33] shows that the ambient signal level will almost always be above  $-90$  dBm. According to [33], planning a DAB network with a carrier frequency of 200 MHz in such a way that DAB service is available in 90 % of the area in a rural area requires a minimum median equivalent field strength of 38.64 dB $\mu$ V/m [33, Table 24]. Assuming that the backscatter device has an antenna gain of 2.15 dBi, this value relates to a received ambient signal power at the backscatter device of  $-82.6$  dBm.

Fig. 9 shows the theoretical limits for the data rate for backscattering data over a certain transmission distance  $R_{RX}$  for various ambient signal levels. Compared to dedicated source backscattering in monostatic setups, ambient backscattering can - depending on the ambient signal level - achieve much higher data rates. This is particularly the case for large transmission distances, where the ambient signal level will usually be much higher than the dedicated carrier that has to be transmitted over the same distance. Another advantage is, that there are ambient signals at lower frequencies than the frequencies we identified for dedicated source backscattering, which leads to a lower path loss.

#### H. Influence of the Carrier Signal Uptime

Especially in case of ambient scenarios the carrier signal uptime may be limited. Examples are WiFi beacons or reference signals in cellular networks. Typical WiFi access points

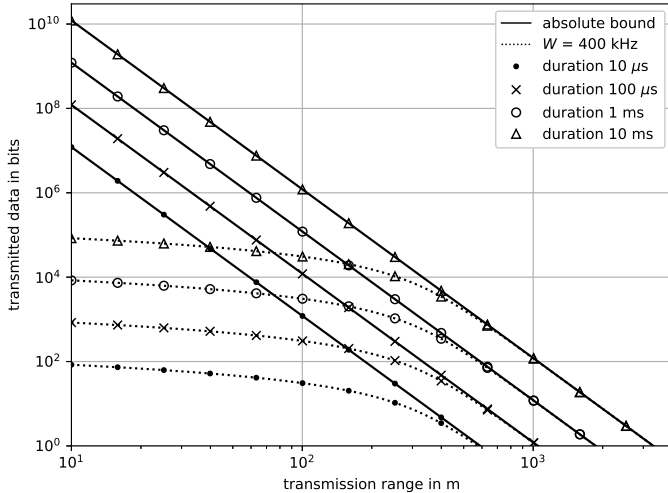


Fig. 10. Maximum number of data bits that can be transmitted in the given carrier signal uptime as a function of the transmission range  $R$ .

transmit beacon signals approx. every 100 ms that have a duration in the order of one to few milliseconds [34]. The 4G cellular standard LTE transmits the Primary and Secondary Reference Signals every 5 ms that have a duration in the order of 130  $\mu$ s [35]. In 5G, the Synchronization Signal Block is typically transmitted every 20 ms and has a duration of  $\approx 285 \mu$ s (for frequency bands  $< 3$  GHz) [35].

Fig. 10 shows the maximum amount of data that can be transmitted within a given signal uptime as function of the transmission range  $R$ . Here, we again assume the mono-static configuration. Already a signal uptime in the order of 1 ms offers the possibility to transmit sufficient number of payload bits. This also holds for the bandwidth limited case with  $W = 400$  kHz.

## V. APPLICATION OF THE BOUND ON UHF-RFID SYSTEMS

We can now use the derived bound to compare them against state-of-the-art UHF-RFID [7] systems. For this purpose we assume a mono-static RFID reader operating according to FCC 15.247 rules [29]: The reader transmits a continuous wave with a transmit power of  $P_C = 28$  dBm. Further, it uses an antenna gain of  $G = 8$  dBi and a carrier frequency of  $f_c = 915$  MHz. This results in the maximum allowed EIRP of 36 dBm (i.e. 4 W). For the backscatter device we use assume a backscatter efficiency of  $\mu = 25\%$  [27], and an antenna gain of  $G_{device} = 2.15$  dBi. Furthermore, we assume the two distances of  $R = 10$  m and  $R = 100$  m. In addition, we use  $F = 20$  dB to represent the losses due to the receiver noise figure (typically high due to full duplex operation), and the transmission of uncoded data bits as UHF RFID does not use a forward error correction code.

We can now use (4) to calculate the received power, and (7) to calculate the maximum rate for the absolute bound. We do not have to calculate the bound for the bandwidth limited case, as this bound will be very close to the absolute bound. This is caused by the high bandwidth of 26 MHz in the regarded frequency range.

TABLE I  
BOUND APPLIED TO UHF-RFID

	$R = 10$ m	$R = 100$ m
$P_{RX}$	-63 dBm	-103 dBm
$C_\infty$	18.2 Mbps	18.2 kbps

Table I shows the resulting values. These are quite close to the values supported by UHF RFID. Using battery assisted RFID transponders a reading range of up to 100 m is supported<sup>2</sup>. The minimum data rate offered by UHF RFID is 5 kbps if Miller-8 encoding is used [7], and hence smaller than the bound of  $C_\infty = 18.2$  kbps for  $R = 100$  m. In contrast, the highest rate offered by UHF RFID is 640 kbps, which is smaller than the bound of  $C_\infty = 18.2$  Mbps for  $R = 10$  m. In summary, these calculated values fit quite well to real UHF RFID backscatter systems.

## VI. SUMMARY AND CONCLUSIONS

Within this paper we developed theoretical capacity bounds for backscatter communications. After defining the backscatter channel model we developed the theoretical bounds based on classical information theory. We especially analyzed the impact of the transmission power, the antenna gains, the carrier frequency, and the system configuration on the achievable maximum data rates in backscatter scenarios. The results show that backscatter communication is able to support high data rates at relevant transmit ranges. We have also shown that the maximum signal bandwidth is an important factor in case of higher signal levels.

Backscatter communication is able to achieve payload data rates in the order of several Mbps. Additionally, also long-range communication over hundreds of meters is possible, but with significantly lower payload data rates. One main limiting factor is the frequency regulation that limits the maximum transmit power for the carrier signals if license-exempt frequency bands are used. Finally, we have shown that our theoretical bounds predict the performance of state-of-the-art UHF RFID systems.

Within the scope of this work we have not made any assumption on the modulation, with the exception of the total bandwidth. Therefore, our future work will focus on efficient backscatter waveform designs that are able to exploit the theoretical capacities as close as possible.

## ACKNOWLEDGMENT

This work is part of the research project 5G-Flexi-Cell (grant no. 01MC22004B) funded by the German Federal Ministry for Economic Affairs and Climate Action (BMWK) based on a decision taken by the German Bundestag.

## REFERENCES

- [1] R. Torres, R. Correia, N. B. Carvalho, S. Daskalakis, G. Goussetis, Y. Ding, A. Georgiadis, A. Eid, J. Hester, and M. M. Tentzeris, "Backscatter communications," *IEEE Journal of Microwaves*, vol. 1, no. 4, pp. 864–878, 2021.
- [2] C. Xu, L. Yang, and P. Zhang, "Practical backscatter communication systems for battery-free internet of things: A tutorial and survey of recent research," *IEEE Signal Processing Magazine*, vol. 35, no. 5, pp. 16–27, 2018.

<sup>2</sup><https://www.impinj.com/products/technology/how-can-rfid-systems-be-categorized> (accessed Dec. 02, 2022)



- [3] I. F. Akyildiz, A. Kak, and S. Nie, "6G and beyond: The future of wireless communications systems," *IEEE Access*, vol. 8, pp. 133 995–134 030, 2020.
- [4] S. J. Nawaz, S. K. Sharma, B. Mansoor, M. N. Patwary, and N. M. Khan, "Non-coherent and backscatter communications: Enabling ultra-massive connectivity in 6g wireless networks," *IEEE Access*, vol. 9, 2021.
- [5] K. Finkenzeller, *RFID Handbook: Fundamentals and Applications in Contactless Smart Cards, Radio Frequency Identification and Near-Field Communication*, 3rd ed. John Wiley & Sons, Ltd, 2010.
- [6] R. Correia and N. B. Carvalho, "Ultrafast backscatter modulator with low-power consumption and wireless power transmission capabilities," *IEEE Microwave and Wireless Components Letters*, vol. 27, no. 12, pp. 1152–1154, 2017.
- [7] "Class-1 Generation-2 UHF RFID Protocol for Communications at 860 MHz - 960 MHz," EPC Global, 2016.
- [8] N. Van Huynh, D. T. Hoang, X. Lu, D. Niyato, P. Wang, and D. I. Kim, "Ambient backscatter communications: A contemporary survey," *IEEE Communications Surveys & Tutorials*, vol. 20, no. 4, pp. 2889–2922, 2018.
- [9] C. Yang, J. Gummeson, and A. Sample, "Riding the airways: Ultra-wideband ambient backscatter via commercial broadcast systems," in *IEEE INFOCOM 2017 - IEEE Conference on Computer Communications*, 2017, pp. 1–9.
- [10] V. Talla, M. Hessar, B. Kellogg, A. Najafi, J. R. Smith, S. Gollakota, and P. G. Allen, "LoRa backscatter: Enabling the vision of ubiquitous connectivity," *Proc. ACM Interact. Mob. Wearable Ubiquitous Technol.*, vol. 1, 2017.
- [11] S. Chen, M. Zhang, J. Zhao, W. Gong, and J. Liu, "Reliable and practical Bluetooth backscatter with commodity devices," *IEEE/ACM Transactions on Networking*, vol. 29, pp. 1717–1729, 8 2021.
- [12] A. Wang, V. Iyer, V. Talla, J. R. Smith, and S. Gollakota, "FM backscatter: Enabling connected cities and smart fabrics," in *14th USENIX Symposium on Networked Systems Design and Implementation (NSDI 17)*. Boston, MA: USENIX Association, mar 2017, pp. 243–258.
- [13] S.-N. Daskalakis, J. Kimionis, A. Collado, M. M. Tentzeris, and A. Georgiadis, "Ambient fm backscattering for smart agricultural monitoring," in *2017 IEEE MTT-S International Microwave Symposium (IMS)*, 2017, pp. 1339–1341.
- [14] R. Torres, R. Correia, and N. B. Carvalho, "All digital ambient backscatter system," in *2020 IEEE Wireless Power Transfer Conference (WPTC)*, 2020, pp. 327–330.
- [15] H. Hwang, R. B. Nti, and J.-H. Yun, "Spectro-temporal combining in bistate WiFi backscatter communication with frequency shift," *IEEE Access*, vol. 9, pp. 113 735–113 747, 2021.
- [16] B. Kellogg, A. Parks, S. Gollakota, J. R. Smith, and D. Wetherall, "Wi-Fi backscatter: Internet connectivity for rf-powered devices," in *Proceedings of the 2014 ACM Conference on SIGCOMM*, ser. SIGCOMM 2014. New York, NY, USA: Association for Computing Machinery, 2014, pp. 607–618.
- [17] Q. Wang, S. Chen, J. Zhao, and W. Gong, "Rapridrider: Efficient WiFi backscatter with uncontrolled ambient signals," in *IEEE INFOCOM 2021 - IEEE Conference on Computer Communications*, 2021, pp. 1–10.
- [18] M. A. ElMossallamy, Z. Han, M. Pan, R. Jäntti, K. G. Seddik, and G. Y. Li, "Backscatter communications over ambient OFDM signals using null subcarriers," in *2018 IEEE Global Communications Conference (GLOBECOM)*, 2018, pp. 1–6.
- [19] G. Yang, Y.-C. Liang, R. Zhang, and Y. Pei, "Modulation in the air: Backscatter communication over ambient OFDM carrier," *IEEE Transactions on Communications*, vol. 66, no. 3, pp. 1219–1233, 2018.
- [20] B. Park and H.-G. Ryu, "Link budget investigation of ambient backscatter communication," in *2021 IEEE International Conference on Consumer Electronics-Asia (ICCE-Asia)*, 2021, pp. 1–3.
- [21] B. Badihi, A. Liljemark, M. U. Sheikh, J. Lietzén, and R. Jäntti, "Link budget validation for backscatter-radio system in sub-1GHz," in *2019 IEEE Wireless Communications and Networking Conference (WCNC)*, 2019, pp. 1–6.
- [22] R. Duan, R. Jäntti, H. Yigitler, and K. Ruttik, "On the achievable rate of bistatic modulated rescatter systems," *IEEE Transactions on Vehicular Technology*, vol. 66, no. 10, pp. 9609–9613, 2017.
- [23] W. Zhao, G. Wang, R. Fan, L. S. Fan, and S. Atapattu, "Ambient backscatter communication systems: Capacity and outage performance analysis," *IEEE Access*, vol. 6, 2018.
- [24] Y. Ye, L. Shi, X. Chu, and G. Lu, "On the outage performance of ambient backscatter communications," *IEEE Internet of Things Journal*, vol. 7, no. 8, pp. 7265–7278, 2020.
- [25] L. Shi, R. Q. Hu, Y. Ye, and H. Zhang, "Modeling and performance analysis for ambient backscattering underlying cellular networks," *IEEE Transactions on Vehicular Technology*, vol. 69, no. 6, pp. 6563–6577, 2020.
- [26] Proakis, *Digital Communications 5th Edition*. McGraw Hill, 2007.
- [27] D. Kuester and Z. Popovic, "How good is your tag?: RFID backscatter metrics and measurements," *IEEE Microwave Magazine*, vol. 14, no. 5, pp. 47–55, 2013.
- [28] A. F. Molisch, *Wireless communications*. John Wiley & Sons, 2012.
- [29] FCC. Title 47, 15.247 Operation within the bands 902-928 MHz, 2400-2483.5 MHz, and 5725-5850 MHz.
- [30] ETSI, *Short Range Devices (SRD) operating in the frequency range 25 MHz to 1 000 MHz; Part 2: Harmonised Standard for access to radio spectrum for non specific radio equipment*, EN 300 220-2, Rev. 3.2.1, Jun. 2018.
- [31] —, *Short Range Devices (SRD); Radio equipment to be used in the 1 GHz to 40 GHz frequency range; Harmonised Standard covering the essential requirements of article 3.2 of Directive 2014/53/EU*, EN 300 440, Rev. 2.2.1, Jul. 2018.
- [32] S. Dolinar, D. Divsalar, and F. Pollara, "Code Performance as a Function of Block Size," *Telecommunications and Mission Operations Progress Report*, vol. 133, pp. 1–23, Jan. 1998.
- [33] *Tech 3391 - Guidelines for DAB Network Planning*, European Broadcasting Union, Brussels, Belgium, May 2018. [Online]. Available: <https://tech.ebu.ch/docs/tech/tech3391.pdf>
- [34] E. Perahia and R. Stacey, *Next generation wireless LANs: 802.11 n and 802.11 ac*. Cambridge university press, 2013.
- [35] E. Dahlman, S. Parkvall, and J. Skold, *5G NR: The Next Generation Wireless Access Technology*. Elsevier Science, 2018.



**Clemens Korn** received the B.Sc. and M.Sc. degree in Electrical Engineering from Friedrich-Alexander University Erlangen-Nuremberg in 2015 and 2017, respectively. In 2017 he joined Fraunhofer IIS, where he conducted research and various industry projects with focus on UHF-RFID and other IoT Systems. Further, he was involved in 3GPP standardization for Fraunhofer IIS as RAN1 delegate for the RedCap study item. In 2021, he started a doctorate at TU Ilmenau, where he conducts research on Zero-Energy Communications.



**Joerg Robert** studied electrical engineering and information technology at TU Ilmenau and TU Braunschweig. From 2006 to 2012, he conducted research on the topic of digital television at the Institute of Communications Engineering at TU Braunschweig. Here he was actively involved in the development of DVB-T2, the second generation of digital terrestrial television. In 2013, he completed his doctorate at the TU Braunschweig on the topic of "Terrestrial TV Broadcast using Multi-Antenna Systems". In 2012, he moved to the LIKE chair at the Friedrich-Alexander-Universität Erlangen-Nürnberg. One of his research focuses there was LPWAN (Low Power Wide Area Networks) and he led the international standardization of LPWAN within IEEE 802. Since 2021, he is university professor and head of the Group for Dependable Machine-to-Machine Communication at the Department of Electrical Engineering and Information Technology at Technische Universität Ilmenau, Germany.



**Tobias Dräger** studied electrical engineering at the Friedrich-Alexander University Erlangen-Nuremberg, specializing in automation technology/sensor technology. After graduating in 2007, he worked at the Fraunhofer Institute for Integrated Circuits IIS with a focus on RFID technology and its application, embedded hardware and wireless transmission technologies. Since 2018, he is head of the "RFID and inductive sensor systems" group, which, in addition to the topics of embedded hardware, wireless energy and data transmission, LTE-Cat NB1 and RFID, also works on the topic of inductive near-field localization IndLoc®.